ARTICLES

Journal of Semiconductors
(2020) 41, 082005
doi: 10.1088/1674-4926/41/8/082005

Strain tunable band structure of a new 2D carbon allotrope C_{568}

Qiang Gao[1, 2], Hasan Sahin[3], and Jun Kang[2, †]

[1]Institute of Semiconductors, Chinese Academy of Sciences, Beijing 100083, China
[2]Beijing Computational Science Research Center, Beijing 100193, China
[3]Department of Photonics, Izmir Institute of Technology, Izmir, Turkey

Abstract: Recently, C_{568} has emerged as a new carbon allotrope, which shows semiconducting properties with a band gap around 1 eV and has attracted much attention. In this work, the external strain effects on the electronic properties of C_{568} have been studied theoretically through first-principle calculations. The numerical results show that while in-plane uniaxial and biaxial strains both reduces the band gap of C_{568} in case of tensile strain, their effects are quite different in the case of compressive strain. With increasing compressive uniaxial strain, the band gap of C_{568} first increases, and then dramatically decreases. In contrast, the application of compressive biaxial strain up to –10% only leads to a slight increase of band gap. Moreover, an indirect-to-direct gap transition can be realized under both types of compressive strain. The results also show that the optical anisotropy of C_{568} can be induced under uniaxial strain, while biaxial strain does not cause such an effect. These results indicate good strain tunability of the band structure of C_{568}, which could be helpful for the design and optimization of C_{568}-based nanodevices.

Key words: 2D C_{568}; monoelemental 2D atomic crystalline materials; strain effects; electronic structures

Citation: Q Gao, H Sahin, and J Kang, Strain tunable band structure of a new 2D carbon allotrope C_{568}[J]. *J. Semicond.*, 2020, 41(8), 082005. http://doi.org/10.1088/1674-4926/41/8/082005

1. Introduction

The success of graphene have triggered the tide of searching novel two-dimensional (2D) materials with desired properties[1–3]. Graphene have been considered at one time to be ideal building blocks of nanodevices. However, the absence of a band gap in graphene is an inevitable obstacle, which hinders its application in electronic devices such as field-effect transistors[4, 5]. Therefore, searching for new 2D materials with suitable band gaps is essential to the development of next-generation electronic devices in nanoscale. A successful example is the discovery of single-layered transition metal dichalcogenides (TMDs). They exhibit distinct properties compared with their bulk counterparts, which broaden our knowledge in 2D materials and are promising for device applications[6–8]. Before long, phosphorene is fabricated and found to be a potential material in the electronic and optoelectronic applications, due to its semiconducting character and high carrier mobility[9, 10]. In recent years, the study on monoelemental 2D atomic crystalline materials have become cutting-edge in the international materials research[11, 12]. Many monoelemental 2D atomic crystalline materials, such as silicene, germanene, stanene, tellurene, have been prepared experimentally and show potential in design of optoelectronic and spintronic devices[13–16]. Moreover, they have the ability to make up for the zero-gap obstacle of graphene and extend the application in electronic devices. Meanwhile, many new carbon structures have been come up, such as phagraphene[17], T-graphene[18], graphyne[19, 20], graphdiyne[21, 22], graphenylene[23], pentagraphene[24], tetrahexcarbon[25], which have enriched the family of monoelemental 2D atomic crystalline materials.

Recently, a new 2D carbon allotrope named C_{568} has been predicted, which is composed of 5, 6, and 8-membered rings of carbon[26]. It is a semiconductor and with an indirect band gap of 1.13 eV. Both phonon spectra and molecular dynamics calculations reveal its stability even at room temperature. Moreover, the researchers show that C_{568} possesses many good intrinsic properties. It is found to be more stable than many other predicted carbon allotropes like T-graphene, T-carbon, and pentagraphene. It also exhibits higher mobility (~10^4 $cm^2V^{-1}s^{-1}$) than black phosphorus monolayer, which make the C_{568} a potential candidate in fabrication of high-performance nanodevices[26]. In this work, we have theoretically studied the external strain effect on the electronic structures of C_{568} through first-principle calculations. In-plane uniaxial and biaxial strains have been considered. The calculations show that the electronic structures exhibit different features under in-plane uniaxial and biaxial strains. When compressive uniaxial strain is applied, the band gap of C_{568} increases first, and then decreases dramatically. However, for biaxial strain, the band gap only increases slowly when C_{568} is compressed up to –10%. Moreover, the compressive strain can change C_{568} from an indirect-gap semiconductor to a direct-gap one. It also shows that uniaxial strain can induce optical anisotropy in C_{568}. These findings show that strain can be an effective way to modulate the electronic properties of C_{568}, which could be helpful for the design of C_{568}-based electronic and optoelectronic devices.

2. Computational methods

The electronic structures of C_{568} are calculated through density functional theory, which is realized in the Vienna *ab initio* Simulation Package (VASP)[27]. The generalized gradient approximation (GGA) of Perdew–Burke–Ernzerhof (PBE)[28]

Correspondence to: J Kang, jkang@csrc.ac.cn
Received 29 MAY 2020; Revised 24 JUNE 2020.

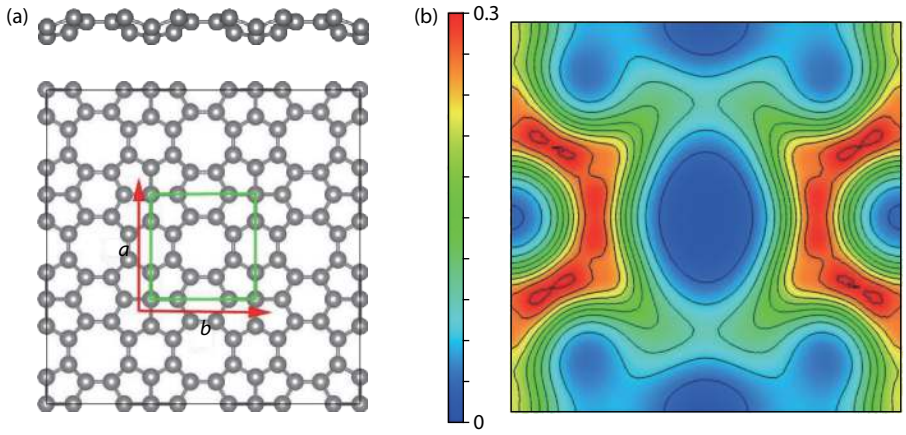

Fig. 1. (Color online) (a) The crystalline structures and (b) 2D charge density difference plot of C_{568}. The square unit-cell marked in green line, where *a* and *b* represent unitcell vectors.

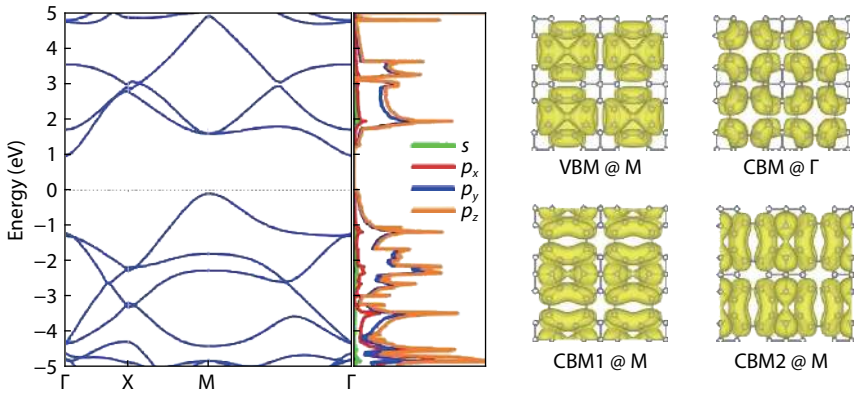

Fig. 2. (Color online) The band structures and projected density of states of C_{568}, with the Fermi level are set to zero. The charge densities of several key states are also presented.

is chosen as the exchange-correlation functional. The method of projected augmented wave potential (PAW) is adopted, with the plane wave cut-off set to be 450 eV[29]. Due to the unsatisfied performance of PBE on predicting the band gap, the Heyd–Scuseria–Ernzerhof (HSE06) functional is also used (with the PBE-relaxed structure) to accurately compute the electronic band structures of C_{568}[30] and to study the strain effect. The Monkhorst–Pack *k*-mesh of 11 × 11 × 1 is selected to sample the Brillouin zone[31]. The Blöch correction is adopted to calculate the density of states of C_{568}. The isolated monolayer C_{568} is simulated by adding a vacuum space of 20 Å into the supercell. The convergence criterion of force and energy are set to be 0.01 eV/Å and 10^{-5} eV, respectively, in the structure optimization. The optical absorption coefficient is calculated through the equation of $\alpha(\omega) = \sqrt{2}\omega[\sqrt{\varepsilon_1^2(\omega)+\varepsilon_2^2(\omega)}-\varepsilon_1(\omega)]^{\frac{1}{2}}$, the $\varepsilon_1(\omega)$ and $\varepsilon_2(\omega)$ are the real part and imaginary part of the dielectric function, respectively. The effective mass of carrier is calculated through quadratic fitting on the conduction band minimum and valence band maximum through the formula[32]: $m^* = [\partial^2 E(k)/\partial^2 k]^{-1}$.

3. Results and discussion

3.1. The crystalline structure and electronic structures of C_{568}

To study the electronic structures of C_{568}, the crystalline structure of C_{568} has been optimized (Fig. 1(a)).

As seen, C_{568} is formed of 5-, 6-, and 8-membered rings, which are composed of sp^2- and sp^3-hybridized carbon atoms. Different from sp^2 hybridized graphene, the carbon rings in C_{568} are not in the same plane, due to the presence of sp^3-hybridization. C_{568} possesses a space group of P-4m2(115) with tetragonal lattice. The optimized C_{568} unit cell contains 13 carbon atoms with lattice parameters of $a = b = 5.725$ Å, which is consistent with the values reported in a recent work[26]. The 2D charge density isosurfaces of C_{568} are also calculated in Fig. 1(b). The covalent bonds are formed between the carbon atoms in the same carbon ring. Moreover, the bond lengths in 5-, 6-, and 8-membered rings are (1.557, 1.447, 1.414 Å), (1.414, 1.403 Å) and (1.447, 1.403 Å), respectively, which indicate the strongest covalent bond is formed in the 6- and 8-membered rings.

The electronic band structure is presented in Fig. 2. The C_{568} possesses an indirect band structure with a band gap of 1.06 eV, which is consistent with the recent work[26]. The conduction band minimum (CBM) is located at the Γ point, whereas the valence band maximum (VBM) is at the M point. The orbital projected density of states shows that the both CBM and VBM are mainly contributed by the p_z orbital states of carbon atoms. Besides the CBM at the Γ point, the conduction band also has a local minimum at the M point, with a two-fold degeneracy. The charge densities of these key states are also presented in Fig. 2. It is interesting to note that the CBMs at the Γ point and the M point exhibit quite different

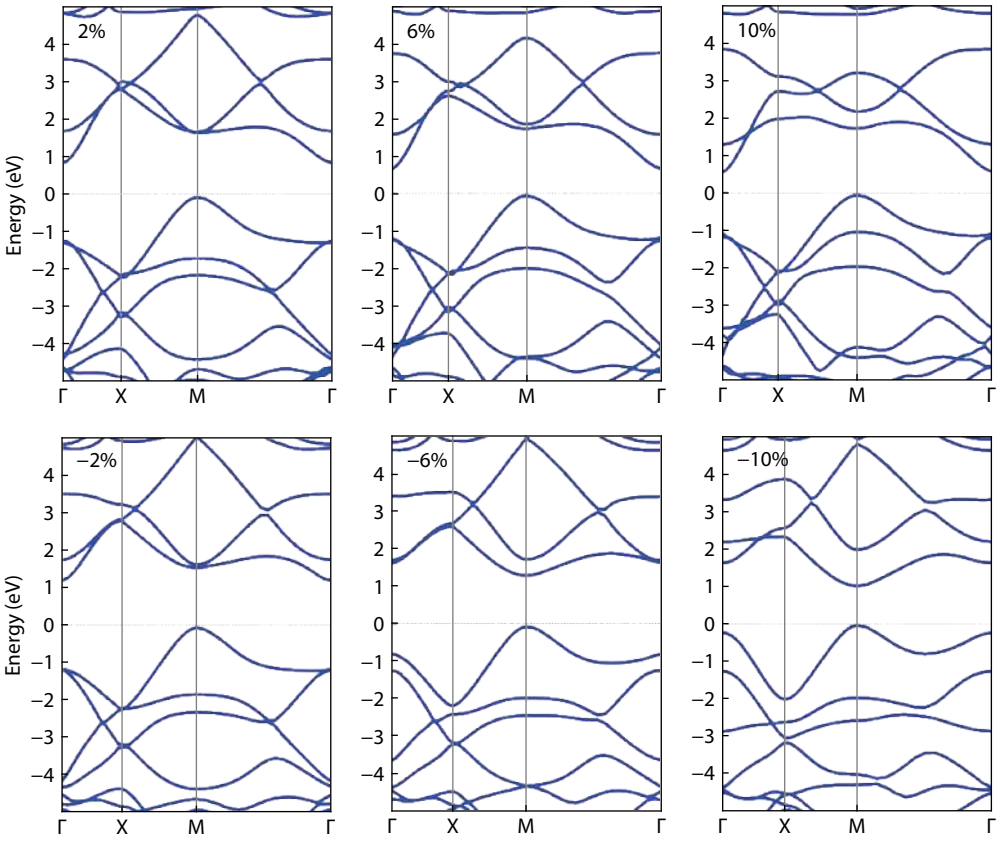

Fig. 3. (Color online) Band structures of C_{568} with different uniaxial strains, with the Fermi level set at zero and marked with the black dashed line. Positive and negative values of strains indicate tensile and compressive cases, respectively.

characters. While the CBM at Γ shows more anti-bonding character, the CBMs at M show more bonding character. The different characters of these states can lead to distinct strain response as will be discussed in the following.

3.2. The external strain effects

External strain is one of the most common effects in the practical applications of materials, which can significantly modify the electronic properties of materials. To understand possible effects of the external strain effect on the electronic properties of C_{568}, we have considered in-plane uniaxial strain and biaxial strain. Through calculations, three unique properties have been found: 1) an indirect-to-direct band gap transition occurs under compressive strain; 2) uniaxial strain and biaxial strain have different effects on the band gap of C_{568}; and 3) uniaxial can induce large optical anisotropy, while biaxial strain cannot. In the following sections, these findings are discussed in detail.

The uniaxial strain effect is firstly studied. The electronic band structures with different strain are shown in Fig. 3. When tensile strain is applied, the band structures show indirect character. The locations of the CBM and VBM remain unchanged. Moreover, it can be clearly seen that with increasing tensile strain, the band gap decreases. Under a 10% strain, the band gap is 0.630 eV smaller than that of the equilibrium state. The situation is different when compressive strain is applied. Under a small strain (–2%), the band gap is still indirect. However, when the strain is increased to –6%, the band gap become direct. While the VBM position remains at the M point, the CBM changes from the Γ to the M point. When compressive strain is further enhanced, the direct band structures are still kept. For the direct band gap, the optical transition between VBM and CBM becomes efficient. Electrons can be excited from VBM to CBM without the assistance of lattice phonons, which is very beneficial to the optoelectronic applications. To clearly show the change of band gap, in Fig. 4, we present the evolution of band gap with external uniaxial strain. It can be seen that the band gap of C_{568} decreases with the increasing tensile strain, and the indirect character is preserved. When compressive strain increase from 0 to –4%, the band gap increases, however, it begins to decrease when the compressive strain exceeds –4%, and becomes direct as discussed above.

The transition from the indirect to direct band gap can be understood from the change of band edge positions at different k points with the applications of strain, as shown in Fig. 4(b). The absolute band edge position is calculated through setting the vacuum level (E_{vac}) as the zero energy reference of calculation[33]. Here we look at the evaluation of the VBM at the M point and the CBM at the Γ and the M points. When tensile strain is increased from 0 to 10%, the VBM and CBM_M only exhibit a slight decrease, while the CBM_Γ moves down in energy space rapidly, leading to a reduction of band gap. However, the application of compressed strain is different from the case of tensile strain. The responses of the CBM at the Γ and the M points are quite different. When compressive strain is applied, the energy of VBM is almost unchanged, and CBM_M decreases monotonously as the strain increases, whereas the energy of CBM_Γ increases monotonously. As shown in Fig. 2, the CBM_M has more bonding character whereas the CBM_Γ has more anti-bonding char-

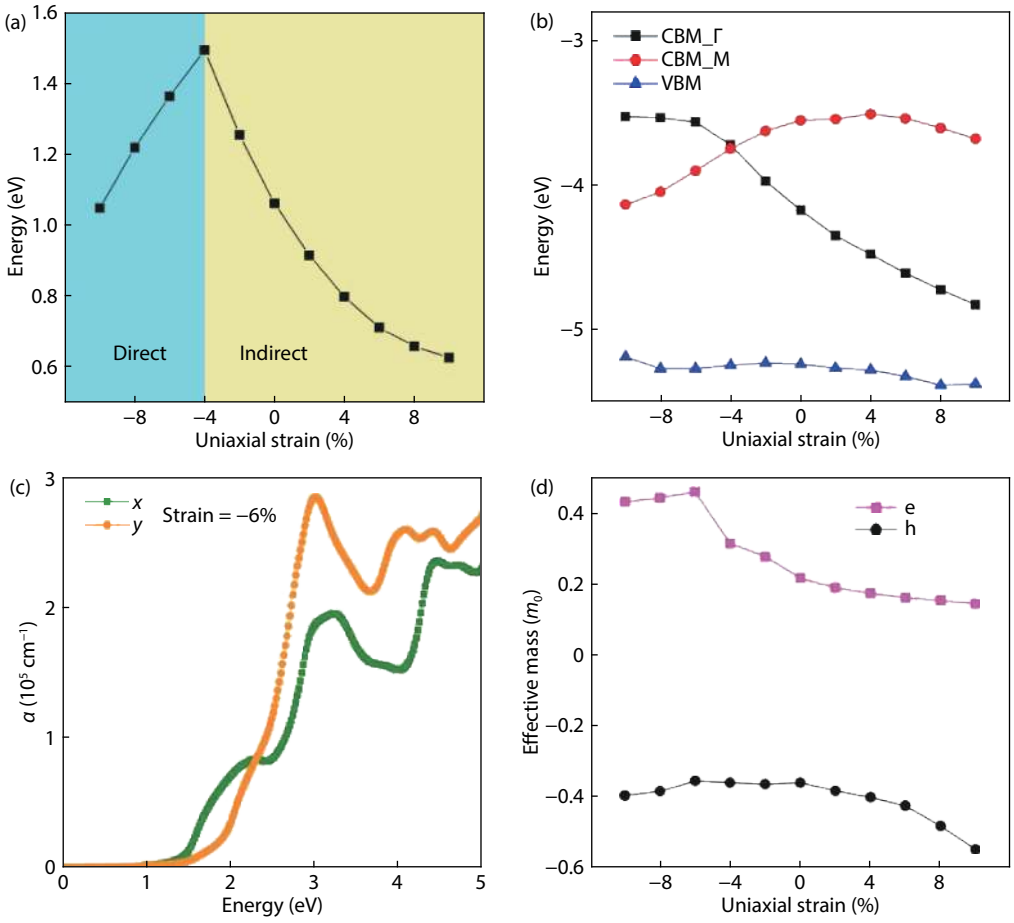

Fig. 4. (Color online) (a) Band gap, (b) band edge position, (c) optical absorption, and (d) effective mass of C_{568} with different uniaxial strains. CBM_Γ and CBM_M are the conduction band minimum at Γ and M points. The vacuum level is taken as the zero energy reference in (b).

acter. Under compression, the distance between atoms is smaller, which lowers the energy of bonding states but increases the energy of anti-bonding states. Thus, the different strain response of the CBM_Γ and CBM_M can be attributed to their different wavefunction characters.

The difference responses lead to a crossover for the CBM_M and CBM_Γ when the compressive strain increases to –4%. Thus, the indirect band structures transform to direct. Moreover, under compressive strain, due to the energy decrease of the CBM_M state, the band gap value decreases when compressive strain is at the range of –4% to –10%.

The optical anisotropy is also a critical factor in design of polarized optoelectronic devices[34]. To examine the anisotropic optical response with the external uniaxial strain, the optical absorption is considered. The optical absorption of C_{568} with the uniaxial strain of –6% is calculated in Fig. 4(c). It is because that the direct band gap can be obtained with the strain of –6%. Thus, the relative high optical absorption can be expected. The calculation shows that the optical absorption is different along *x* and *y* direction, indicating large optical anisotropy. Meanwhile, the optical absorption can reach the order of 10^5. These two optical features indicate that the external uniaxial strain can enhance the optical anisotropy of C_{568}. It is very useful for optical applications, such as polarized photodetectors[35]. The effective mass of charge carriers of C_{568} is also calculated with different uniaxial strain, which is depicted in Fig. 4(d). Apparently, the effective mass of hole and electron decrease with tensile strain. The compressive strain makes the effective masses of hole and electron decrease and increase, respectively. It is because that the tensile strain makes energy bands at the VBM and CBM become flat. For the increase of the effective mass of electron with compressive strain, it can be understood from the change of CBM from Γ point to M point. At the Γ point, the energy band is flat, while at the M point, the energy band is more dispersive. This result indicates that the effective mass of carriers can be modulated through applying external strain, which may be useful for related experiments.

In the following part, the effect of biaxial strain is investigated. We have firstly calculated the band structures of C_{568} with different biaxial strain, which are shown in Fig. 5. For the case of tensile strain, the evaluation of band structures is similar to the case of uniaxial strain. The indirect gap character is intact, and the gap value is smaller under larger stain.

For compressive biaxial strain, the band structures show some difference with the case of uniaxial strain. When compressive biaxial strain increases to –6%, the direct band structures can be obtained, with the both CBM and VBM at the M point. When the compressive strain increases to –10%, the direct band structures become indirect again. Another point can be found that the biaxial does not lift the double degeneracy of CBM at the M point. However, in the case of uniaxial strain, the degeneracy is lifted due to the breaking of symmetry along the two lattice vectors. Thus, the optical trans-

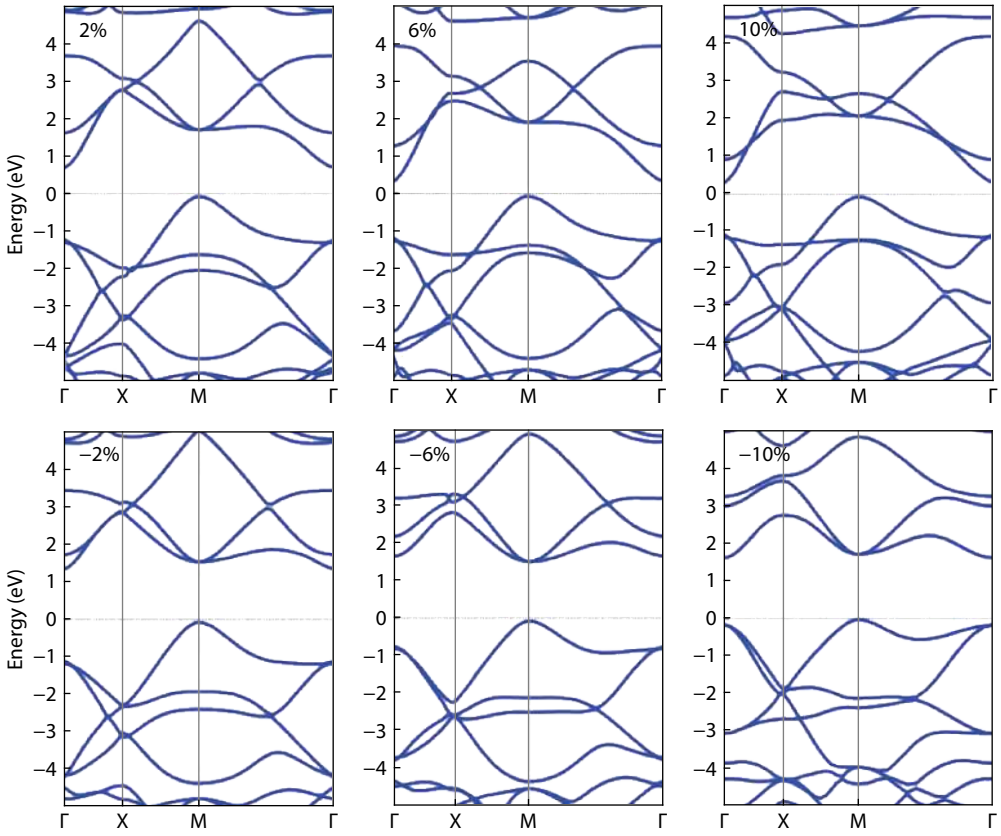

Fig. 5. (Color online) Band structures of C_{568} with different biaxial strains, with the Fermi level set at zero and marked with blacked dashed line. Positive and negative values of strains indicate tensile and compressive cases, respectively.

ition may be different in the case of uniaxial and biaxial strain.

In Fig. 6, we have also calculated the band gap with different biaxial strain. It can be seen that the change of band gap is different from the case of uniaxial strain. When tensile strain is exerted to C_{568}, the band gap keeps dropping. As the tensile strain is enlarged from 0 to 10%, the band gap decreases from 1.062 to 0.380 eV. The trend is the same in the case of uniaxial strain.

However, applying compressive strain from 0 to –10% can make the band gap increase from 1.062 to 1.612 eV, which is different from the case of uniaxial strain. However, applying compressive strain from 0 to –10% can make the band gap increase from 1.062 to 1.612 eV, which is different from the case of uniaxial strain. The tunable range of band gap is 0.381–1.612 eV, which can cover the near-infrared region and visible light region. It indicates that, in the experiment, applying biaxial strain can be effective to control the band gap of C_{568}. It is suitable for the design of optoelectronic devices which can work at near-infrared light or visible light. Further, the band gap keeps direct in the strain range of –4% to –9%, which is desired for the optical performance. To understand the transition from indirect to direct band gap, we also calculate the band edge positions, considering the CBM at the M and the Γ points, as well as the VBM at the M point. We can see from Fig. 6(b) that the CBM_M shifts downwards with increasing compressive strain, and becomes lower than CBM_Γ in the range from –4% to –9%, indicating the conduction band minimum changes from the M to the Γ points. The downward shift is also consistent with the bonding character of CBM_M. Thus, the direct band gap is formed. In addition, in the direct gap region the VBM also shift down with a slightly larger rate compared with the CBM_M, resulting in the tiny increase of the band gap value with enhanced strain. The optical absorption for C_{568} with the strain of –6% is also calculated in Fig. 6(c). The results show that the absorption is isotropic along the *x* and *y* direction, which is different from the optical anisotropy in case of uniaxial strain. It is because uniaxial strain makes the lattice become rectangle. Compared to the square lattice caused by biaxial strain, the lattice symmetry decreases in the rectangle lattice. The decrease of lattice symmetry along *x* and *y* direction renders the optical anisotropy along *x* and *y* direction. The effective mass of hole and electron with the external biaxial strain is also calculated (see Fig. 6(d)). Compared to the effective mass with uniaxial strain, the effective mass for electron and hole is relatively larger.

In experiments, some flexible materials can be the ideal substrate for the growth of 2D C_{568}, such as graphene and plastic substrates. Compressive and tensile strains can be applied on C_{568} by twisting and stretching the substrate. Previous works show that using flexible PVA substrate to encapsulate monolayer 2D material, and twisting soft polymeric substrates with materials are practical ways to modulate the electronic properties of materials and design flexible devices[36–38].

4. Conclusion

Through first-principle calculations, the effect of the external strain on the electronic properties of C_{568} have been in-

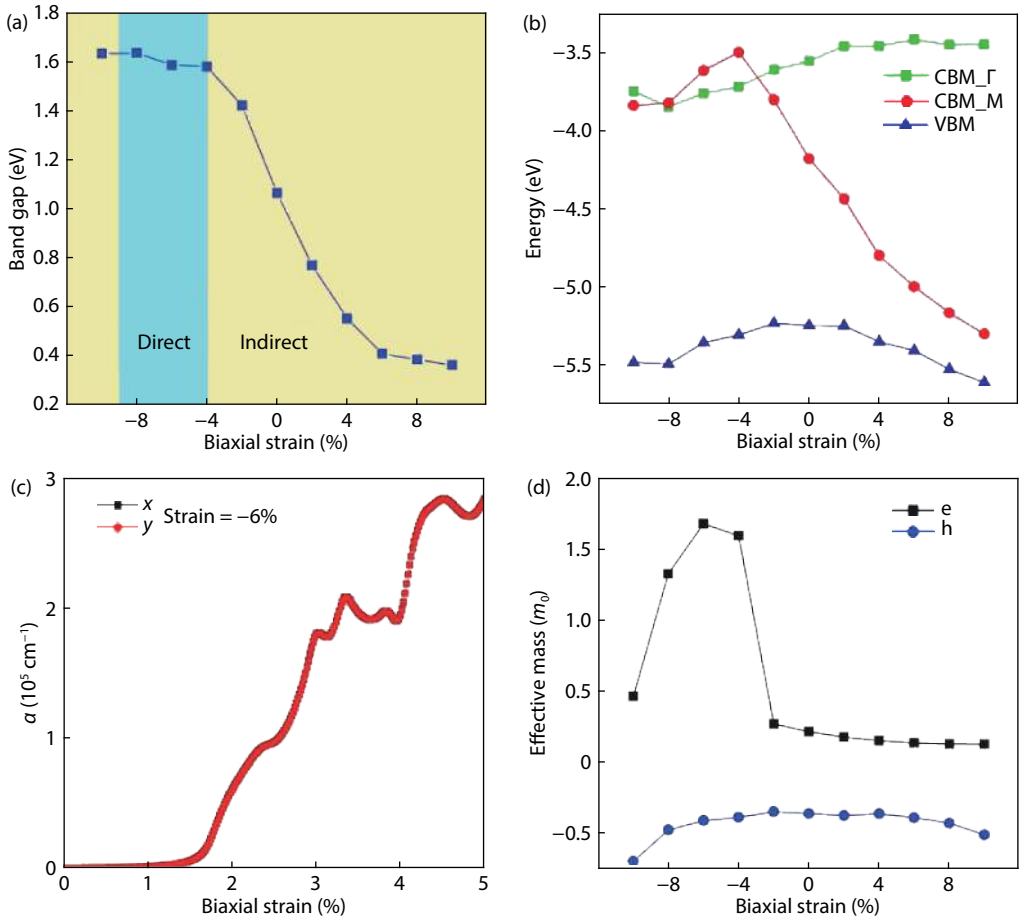

Fig. 6. (Color online) (a) Band gap, (b) band alignment, (c) optical absorption, and (d) effective mass of C_{568} with different biaxial strains. CBM_Γ and CBM_M are the conduction band minimum at Γ and M points. The vacuum level is taken as the zero-energy reference in (b).

vestigated theoretically. The calculations show that while in-plane uniaxial and biaxial strains both reduces the band gap of C_{568} in case of tensile strain, their effects are quite different in case of compressive strain. With increasing compressive uniaxial strain, the band gap of C_{568} first increases, and then dramatically decreases. In contrast, the application of compressive biaxial strain up to –10% only leads to a slight increase of band gap. Moreover, an indirect-to-direct gap transition can be realized under both types of compressive strain. The results also show that the optical anisotropy of C_{568} can be induced under uniaxial strain, while biaxial strain does not cause such an effect. These results could be helpful to experimentally modulate the electronic properties of C_{568}-based nanodevices.

Acknowledgements

This work was supported by NSAF (Grant No. U1930402). Computational resources were provided by Tianhe2-JK at CSRC.

References

[1] Novoselov K S, Geim A K, Morozov S V, et al. Two-dimensional gas of massless Dirac fermions in graphene. Nature, 2005, 438, 197
[2] Ferrari A C, Meyer J C, Scardaci V, et al. Raman spectrum of graphene and graphene layers. Phys Rev Lett, 2006, 97, 187401
[3] Geim A K, Novoselov K S. The rise of graphene. Nat Mater, 2007, 6, 183
[4] Han M Y, Özyilmaz B, Zhang Y B, et al. Energy band-gap engineering of graphene nanoribbons. Phys Rev Lett, 2007, 98, 206805
[5] Zhu W J, Neumayer D, Perebeinos V, et al. Silicon nitride gate dielectrics and band gap engineering in graphene layers. Nano Lett, 2010, 10, 3572
[6] Mak K F, Lee C, Hone J, et al. Atomically thin MoS_2: A new direct-gap semiconductor. Phys Rev Lett, 2010, 105, 136805
[7] Radisavljevic B, Radenovic A, Brivio J, et al. Single-layer MoS_2 transistors. Nat Nanotechnol, 2011, 6, 147
[8] Mak K F, He K, Shan J, et al. Control of valley polarization in monolayer MoS_2 by optical helicity. Nat Nanotechnol, 2012, 7, 494
[9] Li L K, Yu Y J, Ye G J, et al. Black phosphorus field-effect transistors. Nat Nanotechnol, 2014, 9, 372
[10] Reich E S. Phosphorene excites materials scientists. Nature, 2014, 506, 19
[11] Fiori G, Bonaccorso F, Iannaccone G, et al. Erratum: Electronics based on two-dimensional materials. Nat Nanotechnol, 2014, 9, 1063
[12] Xu M S, Liang T, Shi M M, et al. Graphene-like two-dimensional materials. Chem Rev, 2013, 113, 3766
[13] Vogt P, de Padova P, Quaresima C, et al. Silicene: Compelling experimental evidence for graphenelike two-dimensional silicon. Phys Rev Lett, 2012, 108, 155501
[14] Dávila M E, Xian L, Cahangirov S, et al. Germanene: A novel two-dimensional germanium allotrope akin to graphene and silicene. New J Phys, 2014, 16, 095002
[15] Zhu F F, Chen W J, Xu Y, et al. Epitaxial growth of two-dimensional stanene. Nat Mater, 2015, 14, 1020
[16] Zhu Z, Cai X, Yi S, et al. Multivalency-driven formation of Te-based monolayer materials: A combined first-principles and experi-

mental study. Phys Rev Lett, 2017, 119, 106101
[17] Wang Z H, Zhou X F, Zhang X M, et al. Phagraphene: A low-energy graphene allotrope composed of 5-6-7 carbon rings with distorted Dirac cones. Nano Lett, 2015, 15, 6182
[18] Liu Y, Wang G, Huang Q S, et al. Structural and electronic properties of *T*graphene: A two-dimensional carbon allotrope with tetrarings. Phys Rev Lett, 2012, 108, 225505
[19] Baughman R H, Eckhardt H, Kertesz M. Structure-property predictions for new planar forms of carbon: Layered phases containing sp2 and sp atoms. J Chem Phys, 1987, 87, 6687
[20] Narita N, Nagai S, Suzuki S, et al. Optimized geometries and electronic structures of graphyne and its family. Phys Rev B, 1998, 58, 11009
[21] Li G X, Li Y L, Liu H B, et al. Architecture of graphdiyne nanoscale films. Chem Commun, 2010, 46, 3256
[22] Long M Q, Tang L, Wang D, et al. Electronic structure and carrier mobility in graphdiyne sheet and nanoribbons: Theoretical predictions. ACS Nano, 2011, 5, 2593
[23] Song Q, Wang B, Deng K, et al. Graphenylene, a unique two-dimensional carbon network with nondelocalized cyclohexatriene units. J Mater Chem C, 2013, 1, 38
[24] Zhang S H, Zhou J, Wang Q, et al. Penta-graphene: A new carbon allotrope. PNAS, 2015, 112, 2372
[25] Ram B, Mizuseki H. Tetrahexcarbon: A two-dimensional allotrope of carbon. Carbon, 2018, 137, 266
[26] Ram B, Mizuseki H. C568: A new two-dimensional sp2–sp3 hybridized allotrope of carbon. Carbon, 2020, 158, 827
[27] Kresse G, Furthmüller J. Efficient iterative schemes for ab initio total-energy calculations using a plane-wave basis set. Phys Rev B, 1996, 54, 11169
[28] Perdew J P, Burke K, Ernzerhof M. Generalized gradient approximation made simple. Phys Rev Lett, 1996, 77, 3865
[29] Blöchl P E. Projector augmented-wave method. Phys Rev B, 1994, 50, 17953
[30] Heyd J, Peralta J E, Scuseria G E, et al. Energy band gaps and lattice parameters evaluated with the Heyd –Scuseria –Ernzerhof screened hybrid functional. J Chem Phys, 2005, 123, 174101
[31] Monkhorst H J, Pack J D. Special points for Brillouin-zone integrations. Phys Rev B, 1976, 13, 5188
[32] Wang V, Xu N, Liu J C, et al. VASPKIT: A pre- and post-processing program for VASP code. arXiv: 1908.08269, 2019
[33] Kang J, Tongay S, Zhou J, et al. Band offsets and heterostructures of two-dimensional semiconductors. Appl Phys Lett, 2013, 102, 012111
[34] Wang X, Li Y, Huang L, et al. Short-wave near-infrared linear dichroism of two-dimensional germanium selenide. J Am Chem Soc, 2017, 139, 14976
[35] Zhao K, Wei Z M, Jiang X W. Polarized photodetectors based on two-dimensional semiconductors. Sci China Phys Mech Astron, 2019, 63, 1
[36] Li Z, Lv Y, Ren L, et al. Efficient strain modulation of 2D materials via polymer encapsulation. Nat Commun, 2020, 11, 1151
[37] Akinwande D, Petrone N, Hone J. Two-dimensional flexible nanoelectronics. Nat Commun, 2014, 5, 5678
[38] Das S, Gulotty R, Sumant A V, et al. All two-dimensional, flexible, transparent, and thinnest thin film transistor. Nano Lett, 2014, 14, 2861